Available online at www.sciencedirect.com
ScienceDirect
International Journal of Heat and Fluid Flow 28 (2007) 249–261
International Journal of HEAT AND FLUID FLOW
www.elsevier.com/locate/ijhff

Three-dimensional turbulent swirling flow in a cylinder: Experiments and computations

Amit Gupta, Ranganathan Kumar *

Department of Mechanical, Materials and Aerospace Engineering, University of Central Florida, Orlando, FL 32816, USA

Received 26 June 2005; accepted 27 April 2006
Available online 7 July 2006

Abstract

Dynamics of the three-dimensional flow in a cyclone with tangential inlet and tangential exit were studied using particle tracking velocimetry (PTV) and a three-dimensional computational model. The PTV technique is described in this paper and appears to be well suited for the current flow situation. The flow was helical in nature and a secondary recirculating flow was observed and well predicted by computations using the RNG k–ε turbulence model. The secondary flow was characterized by a single vortex which circulated around the axis and occupied a large fraction of the cylinder diameter. The locus of the vortex center meandered around the cylinder axis, making one complete revolution for a cylinder aspect ratio of 2. Tangential velocities from both experiments and computations were compared and found to be in good agreement. The general structure of the flow does not vary significantly as the Reynolds number is increased. However, slight changes in all components of velocity and pressure were seen as the inlet velocity is increased. By increasing the inlet aspect ratio it was observed that the vortex meandering changed significantly.

Keywords: Cyclone; Swirling flow; Turbulence; Particle tracking velocimetry; Renormalization

1. Introduction

Swirling flows are often found in industrial flow applications when intense mixing between different streams is required. A typical example of an application is a swirl-stabilized flame, where the internal recirculating zone acts as a flame holder. Water droplets in petroleum lines and vapor bubbles in cryogenic fluids in microgravity conditions are some other applications in which the two phases need to be separated from the mixture. A common method of inertial separation is cycloning, where particles are separated from a fluid owing to centrifugal forces imparted by a swirling motion of the flow. A conventional cyclone consists of a cylindrical body with a tangential inlet and an axial exhaust called a vortex finder tube. Due to the centrifugal action of the fluid from the tangential inlet, the heavier fluid forms an outer vortex swirling downward through the cone and the lighter fluid forms an inner vortex and exits through the vortex finder tube located at the top. The outflow through the cone is usually called the underflow and that through the vortex finder tube the overflow. If solid particles are to be separated from a liquid phase, then the diameters of the two exhausts would determine the efficiency of separation.

This study concentrates on a single fluid turbulent flow in a cyclone with a tangential inlet and a tangential exit. Such a cylindrical cyclone is not typical since cyclones are usually equipped with a conical portion attached to the cylinder and the exit is normally axial. But a few cylindrical cyclones of the type described here have been used to separate liquid mixtures. For instance, cryogenic liquid transfer in space is difficult since the vapor bubbles caused by heat leaks are dispersed throughout the storage tank. One solution is to use these storage tanks as cylindrical cyclones. This could be done by installing tangential inlet and outlet ports and spinning the liquid and venting the vapor into the atmosphere. In short, the cylinder under

* Corresponding author. Tel.: +1 407 823 4389; fax: +1 407 823 0208.
E-mail address: rnkumar@mail.ucf.edu (R. Kumar).

0142-727X/$ - see front matter © 2006 Elsevier Inc. All rights reserved.
doi:10.1016/j.ijheatfluidflow.2006.04.005

Nomenclature

A	cylinder aspect ratio
A_{in}	inlet aspect ratio
C_p	non-dimensional pressure $\left(\frac{p-p_{in}}{\rho v_{in}^2/2}\right)$
D	diameter of the cylinder (m)
g	acceleration due to gravity (m/s^2)
h	height of the inlet slot (m)
I	turbulence intensity (m s^{-1}/m s^{-1})
k	turbulence kinetic energy (m^2/s^2)
l	width of the inlet slot (m)
L	length of the cylinder (m)
r	radial distance measured from the cylinder axis (m)
R	radius of the cylinder (m)
Re	Reynolds number
S_{ij}	mean strain-rate tensor (s^{-1})
u	velocity (m/s)
u'	fluctuating velocity (m/s)
U	mean velocity (m/s)
V_{in}	inlet velocity (m/s)
x_i	rectangular Cartesian coordinates (m)
z	coordinate along the length of the cylinder (m)

Greek symbols

α_S	swirl factor
δ	Kronecker delta
ε	turbulence dissipation rate (m^2/s^3)
μ_{t0}	turbulence viscosity without swirl (Pa s)
μ_t	modified turbulence viscosity with swirl (Pa s)
ν	kinematic viscosity (m^2/s)
ν_T	kinematic eddy viscosity (m^2/s)
θ	azimuthal angle (rad)
τ	stress tensor (N/m^2)
Ω	characteristic swirl number

investigation has a tangential underflow and no overflow. Legrand et al. (2000) have done a similar experimental study of the wall shear stress in a turbulent swirling decaying flow induced by means of a tangential inlet in an annular cell. The cylinder under consideration by them had a similar inlet and exit. Jakirilić et al. (2002) in their study have tried to provide an insight into the physics of system rotation and swirl, and have studied their effect on turbulence, within the framework of the Reynolds averaged Navier–Stokes (RANS) approach.

Considerable research has been done in cyclonic flows, but most of the research concentrates on pressure drop, particle size and efficiency of separation (Svarovsky, 1985). For efficient separation, the flow has to be steady. The discharge of the separated particles into the underflow is due to the flow itself, and gravity does not significantly affect separation. Therefore, hydrocyclones do not necessarily have to be operated in a vertical position.

The dynamics of the cylindrical cyclone have not been studied thoroughly so far since most of the industrial cyclones are conical counterflow types. In this paper, the cylindrical cyclone was studied to delineate the usefulness of this design, and to advance the knowledge of three-dimensional enclosed flows. The three-dimensional flow dynamics of the cylindrical cyclone are studied using particle tracking velocimetry (PTV) and compared with the k–ε and the RNG k–ε turbulence numerical models. Parks et al. (2002) had used the Reynolds averaged Navier–Stokes (RANS) equation together with the transport equations for the Reynolds stress and the scalar dissipation of turbulence (RSM) to determine the mean velocity and pressure fields for two frustoconical shaped cyclones in their work. The current investigation is limited to the study of the dynamics of a pure liquid flowing in a cyclone. The study also concentrated on identifying the appropriate turbulence model out of the simple k–ε and the RNG k–ε models that could work better for the case of turbulent swirling flows. The motion of the vortex center inside the cylinder was compared for the cases when the $h/D = 1/16$ and $h/D = 1/8$, where h is the height of the inlet slot parallel to the gravity and D is the diameter of the cylinder, using numerical computations at a fixed Reynolds number.

2. Experimental procedure

The cyclone used was a transparent cylinder with an inside axial length of 40.6 cm (16 in.) and an inside diameter of 20.3 cm (8 in.). The inlet and exit were tangentially located at opposite ends of the cylinder and oriented in such that the flow helix is right-handed. Both inlet and

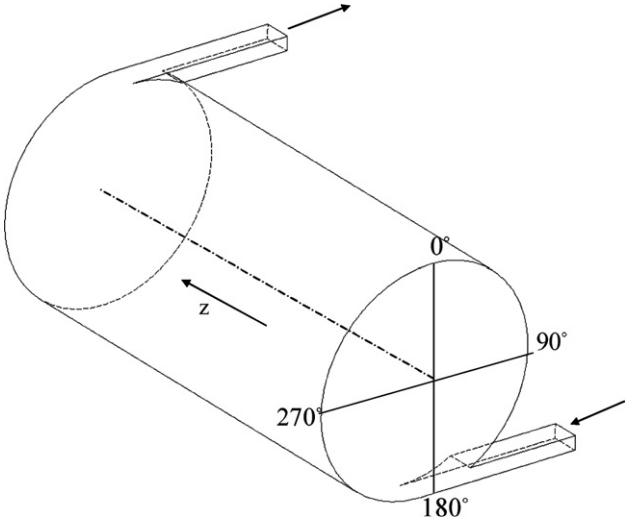

Fig. 1. The cylindrical cyclone with the coordinate system.

the outlet port had rectangular cross-sections and a width of $l = 2.5$ cm (1 in.) and a height of $h = 1.3$ cm (0.5 in.) (see Fig. 1), thus the inlet aspect ratio was $l/h = 2$. Water was pumped through the cylinder in a continuous loop to maintain a steady flow. The cylinder was oriented horizontally with the inlet horizontal and at the bottom. An open settling tank was used to remove air bubbles and the particles were introduced into the cyclone through this settling tank. A throttle valve controlled the flow into the cylinder. In a similar experimental study by Hedlund and Ligrani (2000), local flow behavior and heat transfer characteristics were studied, with particular application in cooling of turbine blades in gas turbine engines. Their setup consisted of two tangential inlet ducts; one at the far extreme on one side and other half way down the length of the cylinder. The exit duct from the cylinder was kept oriented in a radial/axial plane near the end of the swirl chamber location along the cylinder farthest from the inlet ducts. The continuity of mass inflow and outflow was balanced by them by having the exit aspect ratio to be twice of the inlet duct aspect ratio(s).

The primary mode of flow visualization was by illuminating cross-sectional planes of the cylinder perpendicular to its axis. Flow visualization particles illuminated by this plane were then photographed with a SLR camera located along the cylinder axis. A 500 W quartz–halogen lamp with a linear filament was used as the light source. A pair of cylindrical condensing lenses of 44 mm focal length concentrated the light in an image of the filament in the plane of an optical slit. The width of this slit could be adjusted by means of a micrometer screw. Light was then passed through a chopping wheel which is described in the next section. A cylindrical focusing lens of 100 mm focal length then formed an image of the slit at a distance of 900 mm. This lens arrangement minimized the divergence of the light sheet inside the cyclone. The light sheet produced by this optical set up was approximately 3 mm thick at the focal plane near the cylinder axis, slightly diverging cylinder walls. The chopping wheel, its motor, the light and the lens assembly were built into one unit.

2.1. Streak coding

Coded light streaks produce temporal light source modulation during exposure to remove directional ambiguity and in some cases to improve the spatial resolution. The light source is blocked in a unique asymmetrical pattern in time, and the same pattern is reproduced along the length of the streak. This device is illustrated in Fig. 2. The idea is to use a short pulse at each end of the pattern to mark the exact ends of the streak, and to use a long pulse for velocity determination.

As shown in Fig. 2, a chopping wheel was used to block the beam of light inside the plane light projector. The wheel

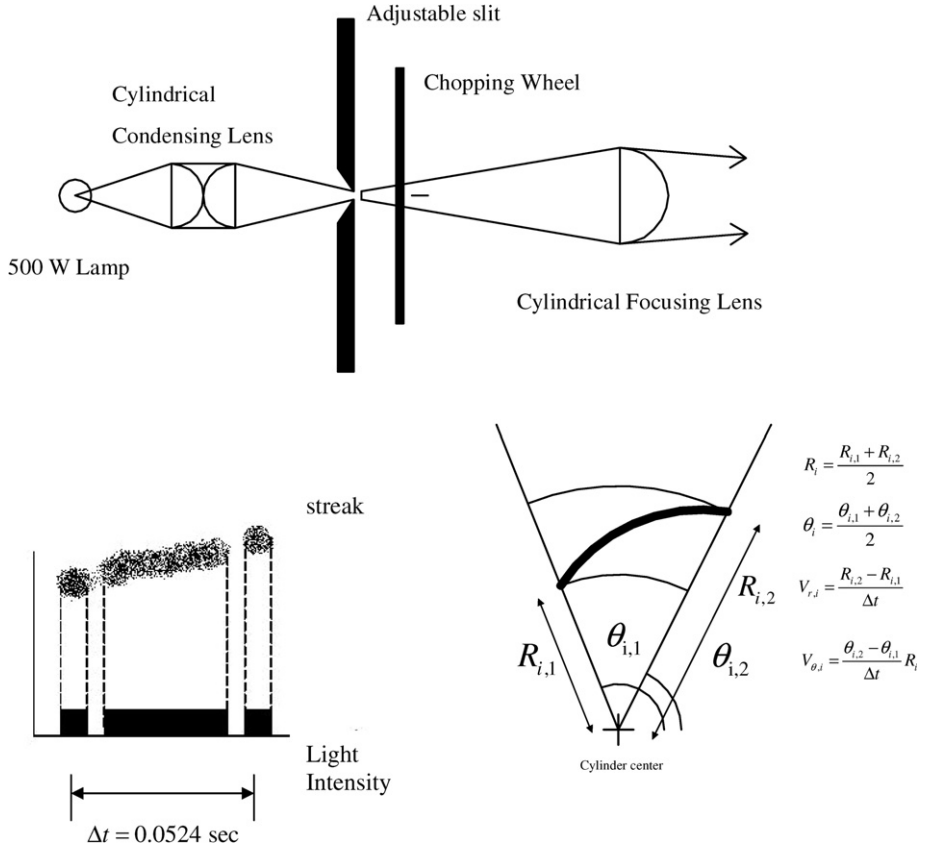

Fig. 2. Diagrams of the light sheet projector with the chopping wheel, and of coded streak formation and velocity measurements.

was made of plexiglass of 1.6 mm (1/16 in.) thickness and 292 mm (11.5 in.) diameter. It was painted black except in transparent wedges to pass the light pulses. The wedges spanned an angular distance of 90° and the wheel rotated at 286 rpm. This translated to a nominal period of 0.0524 s of the streak pattern. This particular pattern featured an initial guard dot, a long gap, a long streak, a short gap and a final guard dot. The camera was aligned with the cylinder axis and photographs were taken with a shutter speed of 1/4 s or less, longer than the wheel rotation time, so that the photographs contained complete streaks.

2.2. Particle tracking velocimetry

The streaks from the moving particles can be measured and, using the streak period of 0.0524 s, the flow velocity could be calculated. This method is called the particle tracking velocimetry (PTV). Non-intrusiveness and simultaneous acquisition of velocities throughout the plane are notable advantages of this method. Imaichi and Ohmi (1983) give a good overview of the theory of PTV and have applied it to the vortex behind a cylinder. Walter (1989) included an extensive state of the art survey of equipment and methods for photographing streaks and measuring them. He created an all-video process by using a CCD video camera to directly photograph his offset channel flow, then storing the digitized image in the computer memory for analysis. Khalighi and Lee (1989) and Mikulec et al. (1988) developed algorithms by which a computer automatically identifies and measures the particle streaks.

An off-line strategy was followed for image analysis. The streaks were first photographed conventionally, then imaged with a CCD video camera and digitized for computer-aided analysis. In spite of the processing delay, this photographic method was preferred since it has better resolution than a video image. An image from Fairchild CCD camera was viewed on the monitor, and then a single frame was digitized and stored by PC vision frame grabber card installed in a personal computer. A video frame was stored as 640×480 pixels at 256 gray scales per pixel. Image processing techniques such as image subtraction and contrast enhancement were used to clean and enhance the images before final analysis.

The PTV measurements in the cylindrical cyclone were based on the coordinate system shown in Fig. 1. With the origin on the inside center of the inlet-end plate, radial distance r was measured from the cylinder axis and the azimuthal angle θ was measured counterclockwise. At the end of image processing, the endpoints of each streak were measured in pixel coordinates, and these coordinates were transformed algebraically into polar coordinates. This transform was recalibrated for each image because of the changing alignments of the camera and photographic processor's enlargements. Streak characterization is given in Fig. 2. The radial and azimuthal location of the streak was calculated as the arithmetic mean of the endpoint radii and azimuthal angles respectively to fix the coordinate. The velocities were then calculated using the streak period. According to the coordinate system, the clockwise velocity would be positive. The coordinate locations and velocities were then stored for sorting and interpolation. The randomly scattered point measurements were interpolated using focal plane fitting using the least squares method.

2.3. Uncertainty in experimental measurements

The location uncertainty in image processing is half a pixel, i.e. 0.2 mm. The length uncertainty in the streaks also introduced uncertainty in velocity measurements. Based on the period of streak, the velocity uncertainty only due to length inaccuracies was estimated to be 8 mm/s. The angular speed of the light-chopping wheel (286 rpm) was calibrated to within 1%. The photographic streaks were obtained a light sheet 3 mm thick. However, no significant error in velocity was anticipated. The terminal velocity of the seeded particles were estimated to be less than 10 mm/s and its effect in quantitative visualization is small. The higher intensity turbulence also kept the particles well mixed in the flow. Finally, there was an inherent error in interpolating velocities by plane fitting the known velocity planes. The direct approach was to use three points forming a triangle with the unknown point inside. The choice of the triangle became an important subjective problem when four or more known points surrounded the unknown point. Sometimes as many as six points were used to obtain a smoother surface.

3. Numerical model

The computational fluid dynamics code, FLUENT, was used to investigate the 3-D swirling, turbulent flow in the cylinder using the standard k–ε and renormalized group k–ε (RNG) turbulence models. The governing partial differential equations for the conservation of mass, momentum, and transport of turbulent kinetic energy and its dissipation were rearranged in a general form, discretized and solved using the control-volume method (Patankar, 1980). Choudhury (1993) has defined a way of modifying the turbulence viscosity to account for the swirl in the flow, which is given by

$$\mu_t = \mu_{t0} f\left(\alpha_S, \Omega, \frac{k}{\varepsilon}\right) \tag{1}$$

where μ_{t0} is the value of turbulent viscosity calculated without the swirl modification, Ω is a characteristic swirl number and α_S is a swirl factor that assumes different values depending upon the magnitude of swirl in the flow. In the present study, a swirl factor of 0.07 was used. A brief description of the k–ε and the RNG k–ε models is given in Appendix A. Referring to Eqs. (A.4) and (A.5) in Appendix A, for the standard k–ε model the closure conditions and auxiliary relations are fixed as

$$C_{\varepsilon_1} = 1.44, \quad C_{\varepsilon_2} = 1.92, \quad C_\mu = 0.09,$$
$$\sigma_k = 1.0, \quad \sigma_\varepsilon = 1.3$$

A more recent version of the k–ε model had been developed by Yakhot and Orszag (1986). They used techniques from the renormalization group theory, and developed what is known as the RNG k–ε model. The essence of the RNG model is that the values of the constants are calculated explicitly. The procedure involves the removal of the smallest scales of turbulence to a point from where on the remaining scales are resolvable with available computing capacities. The eddy viscosity, k and ε are still given by (A.3)–(A.5). However, the model uses a modified coefficient, C_{ε_2} defined by

$$C_{\varepsilon_2} = \widetilde{C}_{\varepsilon_2} + \frac{C_\mu \lambda^3 (1 - \lambda/\lambda_0)}{1 + \beta\lambda^3}$$
$$\lambda = \frac{k}{\varepsilon}\sqrt{2\,S_{ij}S_{ji}} \tag{2}$$

The closure coefficients for the RNG k–ε model are

$$C_{\varepsilon_1} = 1.42, \quad \widetilde{C}_{\varepsilon_2} = 1.68, \quad C_\mu = 0.085, \quad \sigma_k = 0.72,$$
$$\sigma_\varepsilon = 0.72, \quad \beta = 0.012;\ \lambda_0 = 4.38$$

4. Results and discussion

In standard cyclone terminology, the cylinder under investigation had a tangential underflow and no overflow, and thus could be an approximation to a reverse flow cylinder cyclone in which most of the working fluid passes to the underflow. In a companion study of qualitative flow visualization of the same geometry, Kumar and Conover (1993) found that axial symmetry of the flow does not hold in the cylindrical cyclone. Pan (1992) compared the PTV experimental data to the simple k–ε model and found them to be in good agreement. It was also found in his study that using tangential and fully developed exit boundary conditions do not change the structure of the flow, except near the exit plane, and that a considerable flow reversal occurs in the cylinder. Neto et al. (1998) dedicated their study to the numerical modeling of the hydrodynamics of the laminar swirling flow in an annulus. They had used the finite-element method to solve the governing equations.

In the present work, photographs were obtained at various cross-sectional planes along the axis of the cylinder. Although the mean flow is steady, the center of the vortex in each plane rotates randomly about an imaginary axis with an amplitude of less than 12.7 mm. A representative photograph using the light-chopping wheel at $z/D = 0.094$ is given in Fig. 3. The longer streaks close to the cylinder wall indicate that the velocities are higher and the shorter streaks diminishing to dots represent the core of the vortex in that plane. The vortex location in the exit plane was difficult to identify since the large scale turbulence in that plane disrupts the central rotation. The vortex center in the rest of the cross-sections is observed to be stable but steady. The vortex center in each plane rotated around its average location and only the photographs with the vortex center at its average location were chosen for analysis. No ensemble averaging of velocities was done at any axial location.

Photographs at different planes were interpolated, and resulting vector fields are given in Fig. 4 for axial locations of $z/D = 0.75$ and 1.375 respectively. The vortex center is present in the third quadrant for the former case and in the fourth quadrant in the latter. Looking at Figs. 3 and 4, a broad picture of the spiraling motion of the vortex center along the length of the cylinder can be gauged. From these figures it can be observed that the vortex moves from one quadrant into another, crossing the axis of the cylinder, until finally it exits the cylinder. As has been observed previously by Kumar and Conover (1993), the center of vortex appears in the first quadrant at the inlet and meanders around anticlockwise once for the cylinder aspect ratio (L/D) of 2, as it traverses through the length of the cylinder. The entire flow may, thus, be visualized as consisting of two streams, termed as the primary flow and the secondary flow. The flow from the inlet which supplied the mass and angular momentum to the entire flow, also termed the primary flow, quickly fans out from the inlet and rotates around the cylinder in a thin layer. It follows a helical path and is distinct from the secondary flow which it surrounds. Legrand et al. (2000) had similar observations in their study; near the inner wall of the annulus, a recirculating zone developed that followed the main helical motion of the fluid along the flow path and high local velocities were found towards the external wall of the annular cell.

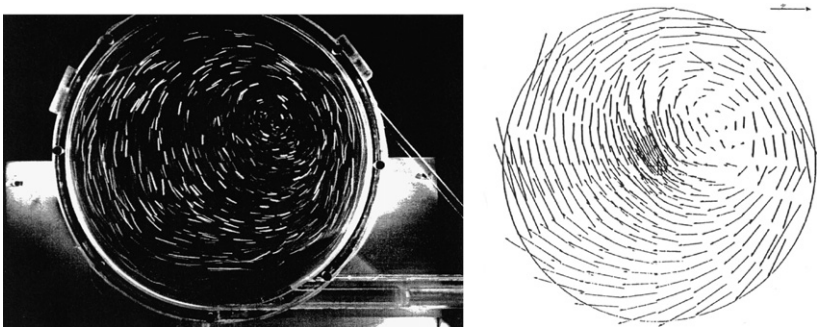

Fig. 3. Photograph of the cyclone taken at $z = 19$ mm, and PTV velocity vectors. Scale arrows are shown for 254 mm/s.

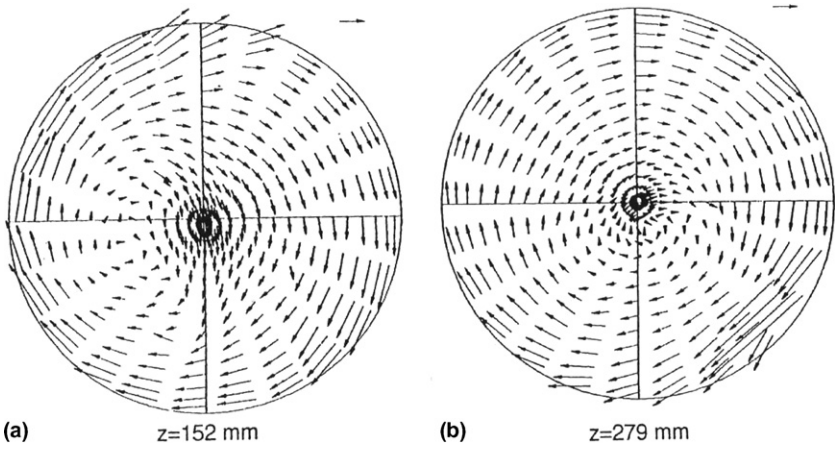

Fig. 4. PTV results for the cross-sections (a) 152 mm, and (b) 279 mm.

For a Reynolds number of 9000, which is defined as $Re = \frac{\rho V_{\text{in}} D_{\text{H}}}{\mu}$, and the geometric parameters given by (L/D) of 2, and the inlet aspect ratios of 2 and 4, tangential velocity vectors were computed and plotted in several cross-sections of the cylinder. The velocity vectors are shown in Figs. 5 and 6 for selected planes along the length of the cylinder. From these figures it can be observed that the secondary recirculation zone moves in a spiraling manner around the cylinder axis on its way to the exit of the cylinder. Looking at these figures, it is understood that the flow structure on each of the planes is quite similar as the vortex core is found to be in the same quadrant when comparing the flow field on the same plane for the two cases, for the same Reynolds number, and for different inlet aspect ratios. It is concluded, thus, that the vortex follows a

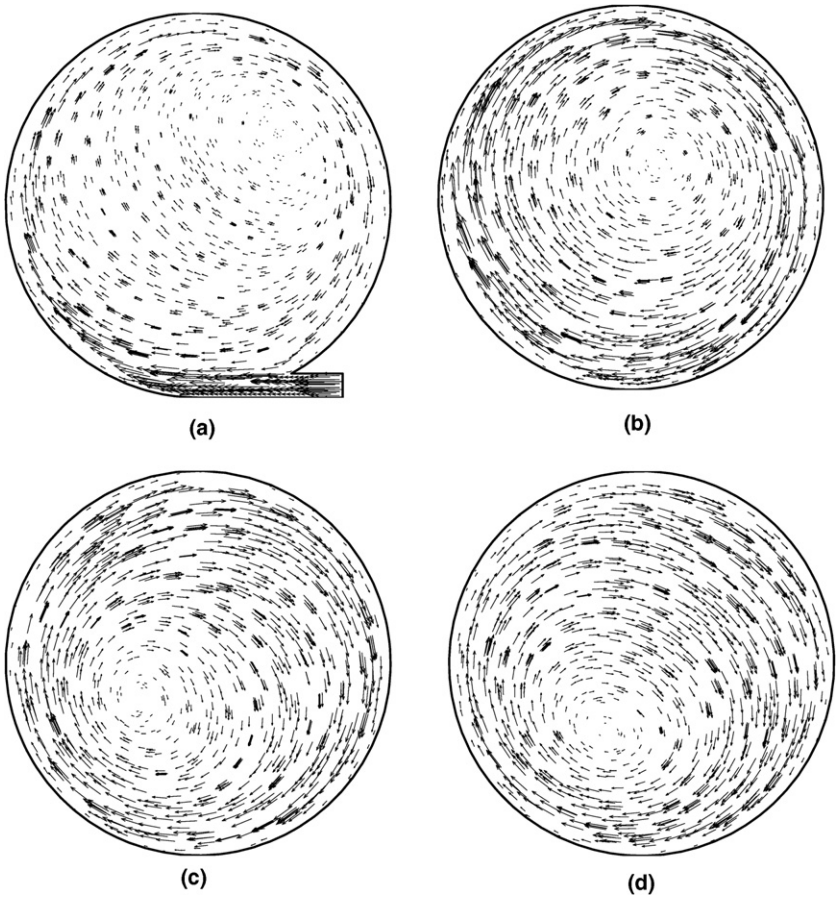

Fig. 5. Tangential velocity profiles at the cross-sections (a) $z/D = 0.094$, (b) $z/D = 0.25$, (c) $z/D = 0.75$, and (d) $z/D = 1.0$ for $Re = 9000$ and an inlet aspect ratio of 2.

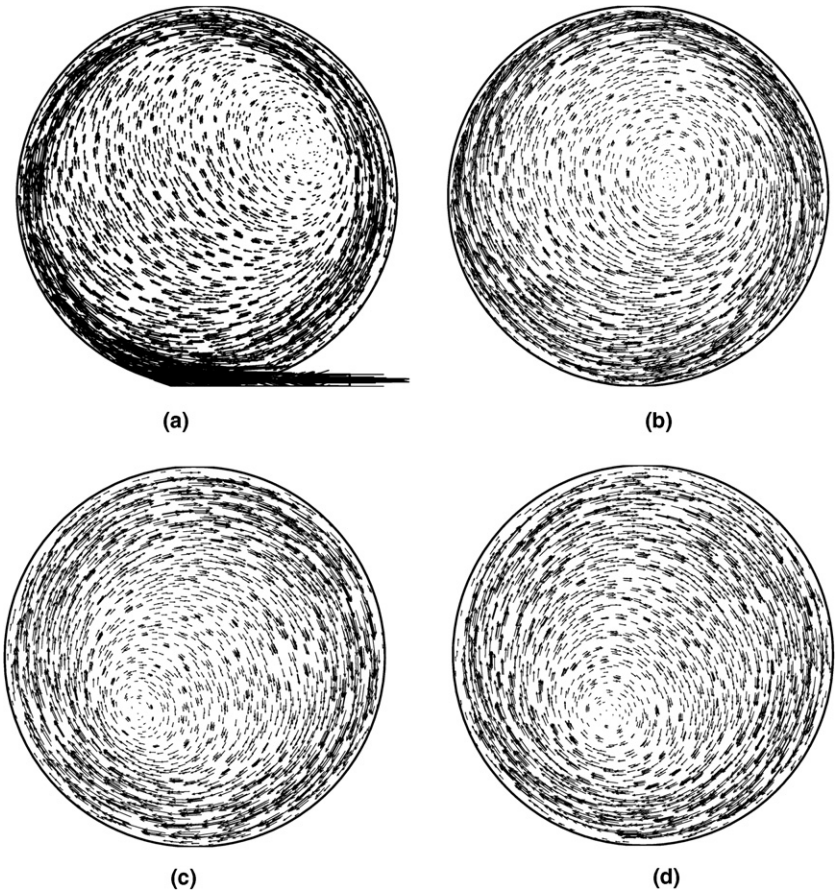

Fig. 6. Tangential velocity profiles at the cross-sections (a) $z/D = 0.094$, (b) $z/D = 0.25$, (c) $z/D = 0.75$, and (d) $z/D = 1.0$ for $Re = 9000$ and an inlet aspect ratio of 4.

similar path, only the coordinates of the vortex center change on changing the inlet aspect ratio.

In order to understand the dynamics of the flow, the pressure field was analyzed along with the tangential velocity profiles for the different inlet aspect ratios at the same Reynolds number. The non-dimensional pressure is plotted in Fig. 7 for an inlet aspect ratio of 2 and 4. The pressure values have been plotted at three planes: very close to the inlet; midway down the length of the cylinder; and close to the exit. The pressure has been normalized by $(\rho V_{\text{in}}^2/2)$. The Reynolds number was fixed at 9000 and the cylinder aspect ratio was 2. It was observed that for a lower inlet aspect ratio, the non-dimensional pressure was higher towards the wall of the cylinder, at times being close to more than twice of the value computed for the higher inlet aspect ratio of 4. At the exit, i.e. $z/D = 1.925$, the normalized pressure is negative. The negative values for the pressure may be explained by the fact that the core of the vortex is close to the line $\theta = 0°$ (see Fig. 1 for the coordinate system used). This implies that the negative pressure zone is close to the location where the vortex core is present. Comparing these pressure profiles with the tangential velocity profiles (Fig. 8) at the same axial locations and for the same Reynolds number, we find some similarities. Portions of the tangential velocity profiles at the inlet and exit are negative, as was the case with the pressure distribution. This is due to the fact that the force due to the radial pressure gradient very nearly balances the centrifugal force. In general, away from the inlet and the exit, the non-dimensional pressure and tangential velocity decrease with an increase in inlet aspect ratio.

4.1. Comparison of experimental and numerical results

Tangential velocity comparison was done for RNG numerical data and the PTV measurements where available. An illustrative comparison is shown in Fig. 9 at an axial location of $z/D = 0.75$ (i.e. $z = 152$ mm). The trend was found to be similar in the variation of the tangential velocity on this plane with the velocity increasing nearly linearly towards the wall and then drops to zero at the wall because of the no-slip wall boundary condition. The parameters used for this comparison were $h/D = 1/16$ i.e. $A_{\text{in}} = 2$; $l/D = 1/8$; $L/D = 2$; $Re = 18{,}000$. The trend in the results is well predicted near the top of the cylinder ($\theta = 0°$) and not so well near the side ($\theta = 90°$). This is not surprising because the vortex center at a plane was observed to be non-stationary and the numerical model could not account for this behavior. In general, considering the RNG k–ε model used and the experimental uncertainty of

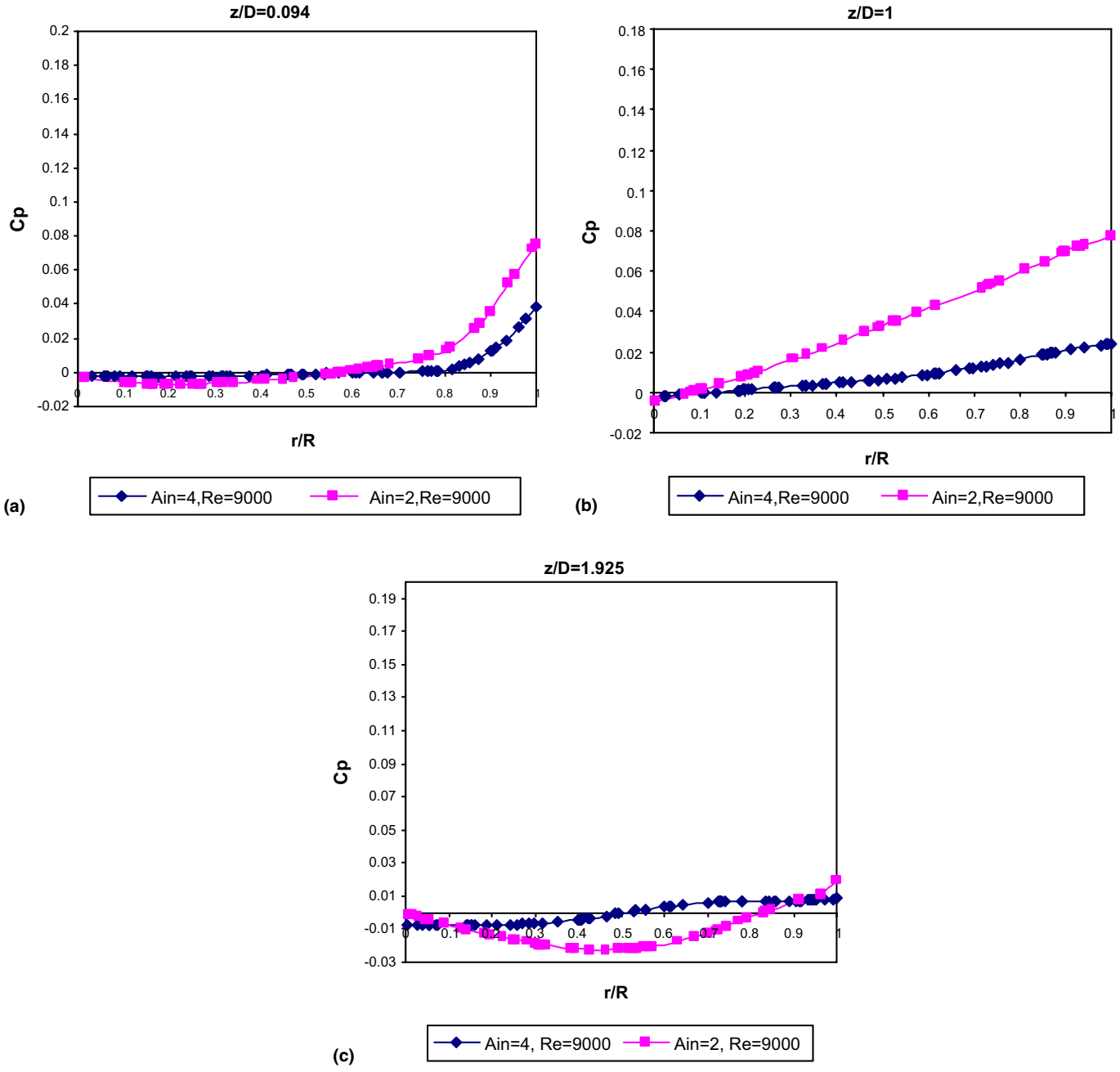

Fig. 7. Pressure comparison for the aspect ratios of 2 and 4 at the planes given by (a) $z/D = 0.094$, (b) $z/D = 1.0$, and (c) $z/D = 1.925$, and $\theta = 0°$ at $Re = 9000$. The non-dimensional pressure is given by $C_p = \frac{(p-p_{in})}{(\rho v_{in}^2/2)}$.

approximately 15%, the numerical results of mean velocity are in good agreement with the experimental results. It is expected, however, that inaccuracies in details of turbulence could occur, as has been encountered by Sharif and Busnaina (1988) and Durst and Wennerberg (1991) who used the simple k–ε turbulence model in confined swirling flows.

Yang and Ma (2003) had investigated the performance of the four cubic eddy-viscosity turbulence models for two strongly swirling confined flows. In their validation which was done for two test cases, the first being a rotating pipe flow and second was a swirling jet flow, they found that the cubic models predicted results that matched well with the experimental data as compared to the standard k–ε model. In our study, it was found that using the standard k–ε turbulence model yielded results that deviated from the experimental data and that the RNG k–ε model produced a better match with the experiments. This is due to the fact that a swirl modification factor is built into the RNG model that enables a better prediction of the simulation of flows with a high swirl. With the standard k–ε model, no such modification was possible.

Jakirilić et al. (2002) have mentioned that the standard k–ε model is not directly sensitive to rotation and swirl

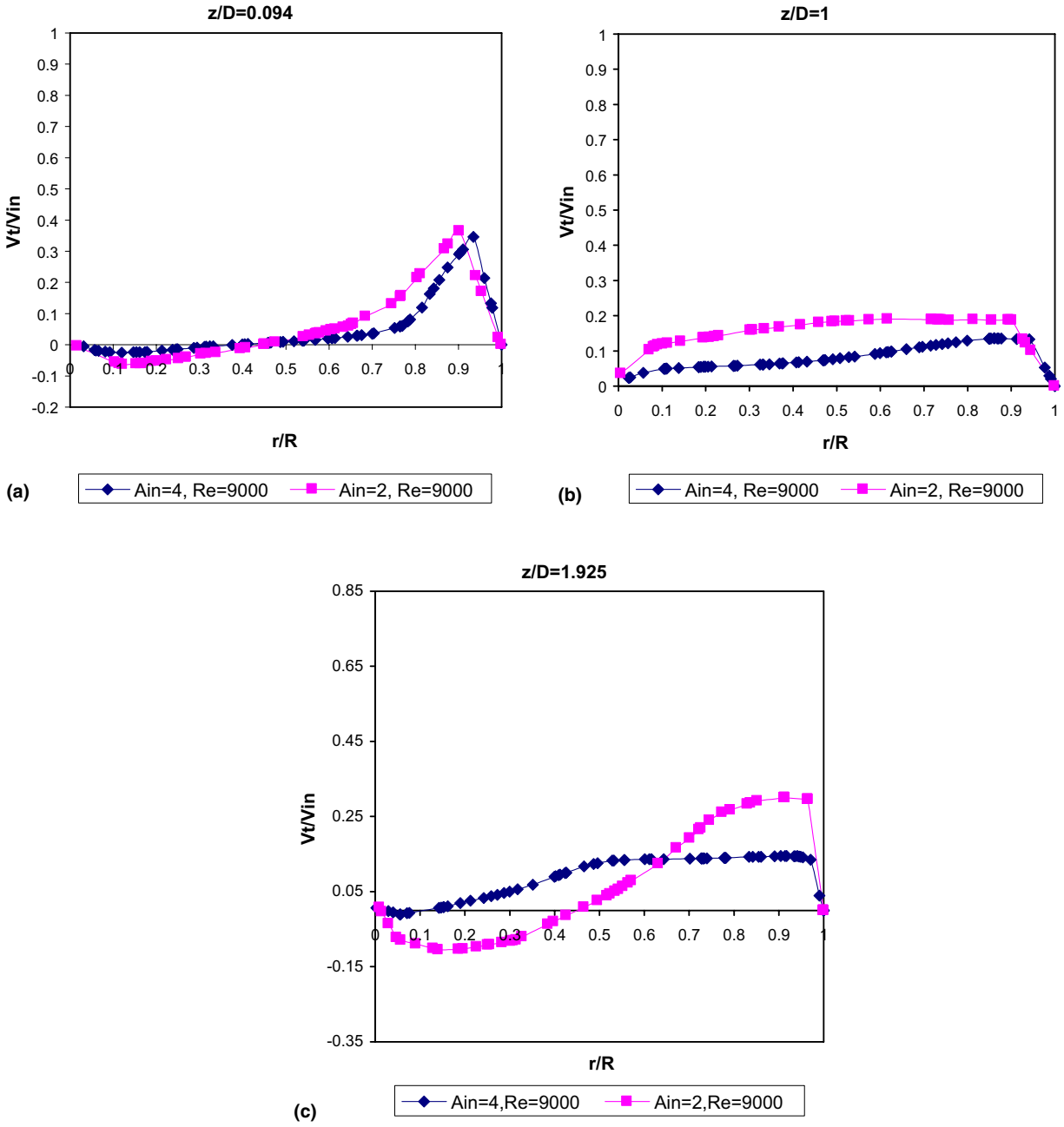

Fig. 8. Tangential velocity comparison for the aspect ratios of 2 and 4 at the planes given by (a) $z/D = 0.094$, (b) $z/D = 1.0$, and (c) $z/D = 1.925$, and $\theta = 0°$ at $Re = 9000$. The non-dimensional velocity is given by v/v_{in}.

flows because of the absence of any specific terms in the equations accounting for these effects. They studied the performance of second-moment closures in a range of rotating and swirling flows. But they assumed that the flow is axi-symmetrical in three-dimensions. In a similar study by Pettersson et al. (1998), second-moment closures were devised to model near-wall effects on rotating pipe flows. They captured the near-wall effects in an axial pipe flow by means of an elliptic relaxation, although with the underlining assumption that the mean flow field is one-dimensional and two-componential so that only two non-zero components of velocity exist. These assumptions have not been used in the current study. In the current flow situation, the maximum error is found to be within 20% and the computational prediction appears to be acceptable to analyze the dynamics of the swirling flow in the cylinder.

Numerical results in different planes suggest, as in our laboratory experiment, that the center of the vortex changes its position around the axis as the flow heads towards the exit. As can be seen in Fig. 10, the vortex centers from the numerical computations using the RNG model have been plotted at different planes perpendicular to the axis of the cylinder and compared with the PTV measurements. The parameters used for this comparison

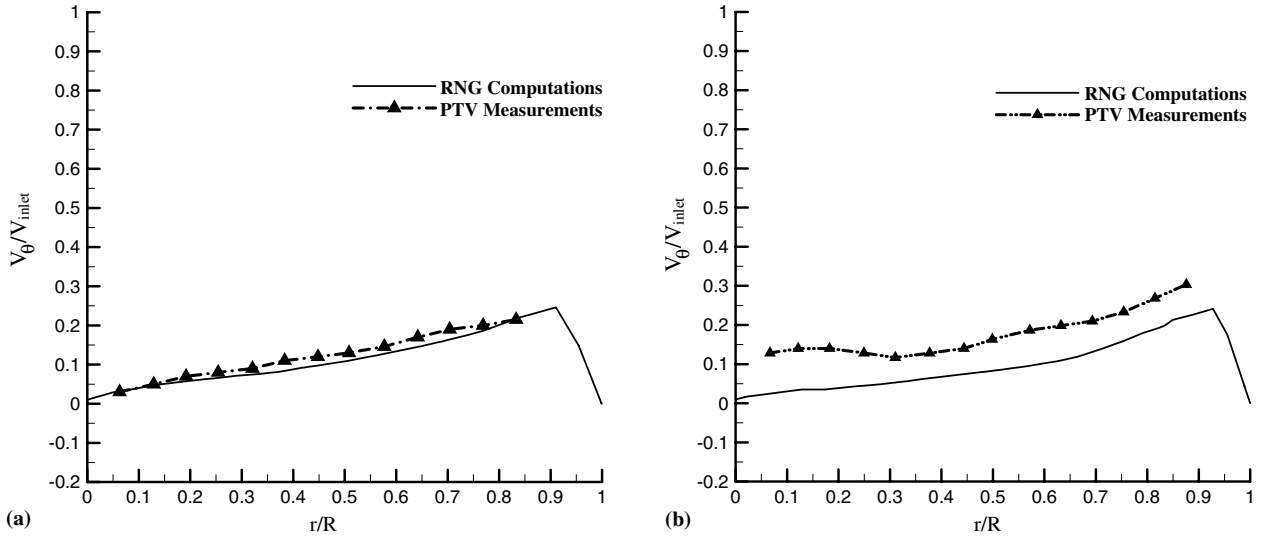

Fig. 9. Comparison of tangential velocity profiles from PTV results and from numerical computations at $z = 152$ mm for (a) $\theta = 0°$, and (b) $\theta = 90°$.

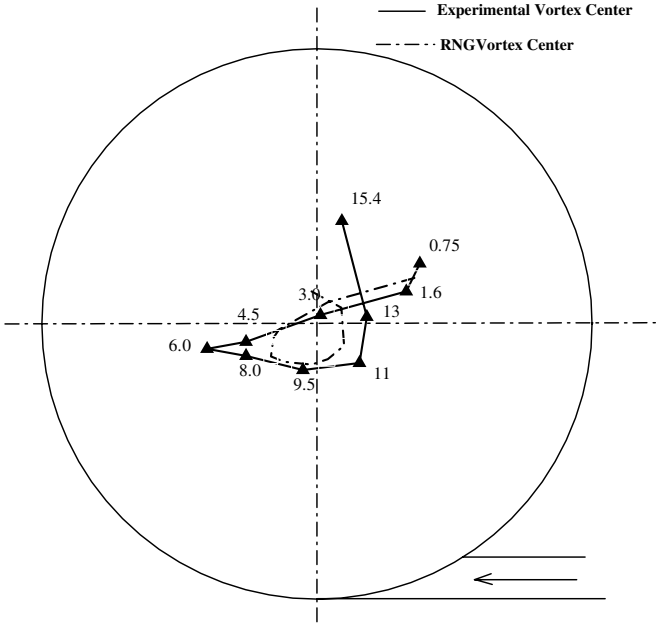

Fig. 10. Locus of the vortex center for inlet aspect ratio of 2 (i.e. $h/D = 1/16$) and $Re = 18{,}000$. Axial coordinates are marked in inches.

were an inlet aspect ratio of 2 (i.e. $h/D = 1/16$) and $Re = 18{,}000$. Quantitatively the experimental results tend to show more migration of the center core compared to the numerical results, especially at the sides where we already noticed a deviation in tangential velocity. Khalighi and Lee (1989), Khalighi (1989) and Mikulec et al. (1988) characterized the in-cylinder swirl flow in an engine during the induction process by means of flow visualization and PTV. Their results cannot be directly compared with the present results due to the difference in geometry. Qualitatively, however, their results revealed the presence of a single vortex with its center of rotation eccentric to the cylinder axis. In addition, Khalighi's (1989) results showed that on each horizontal cross-section plane, the center of rotation tended to rotate about the cylinder axis as it was formed during the intake stroke.

Numerical computations for h/D ratios of 1/16 and 1/8 and $Re = 18{,}000$, using the RNG turbulence model reveal that although the vortex follows a similar path, the locations of the vortex centers are different when observed at planes perpendicular to the z-direction as is shown in Fig. 11. A three-dimensional view of the movement of the core in Fig. 12 shows the meandering of the vortex center, making one complete revolution around the axis, although the vortex axis of rotation is not parallel to the axis of the cylinder, thereby contributing to a strongly three-dimensional flow. To extend the same analysis for comparison of the vortex movement through the cyclone,

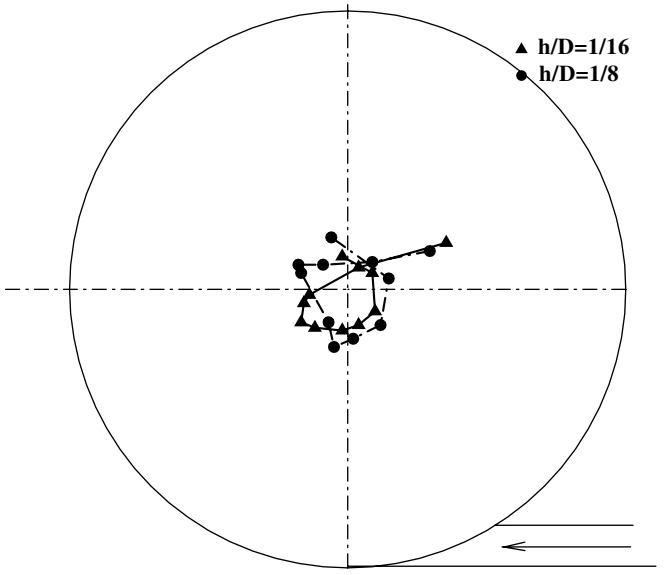

Fig. 11. Locus of vortex centers for different inlet slot height to diameter ratios of $h/D = 1/16$ and $h/D = 1/8$ and $Re = 18{,}000$.

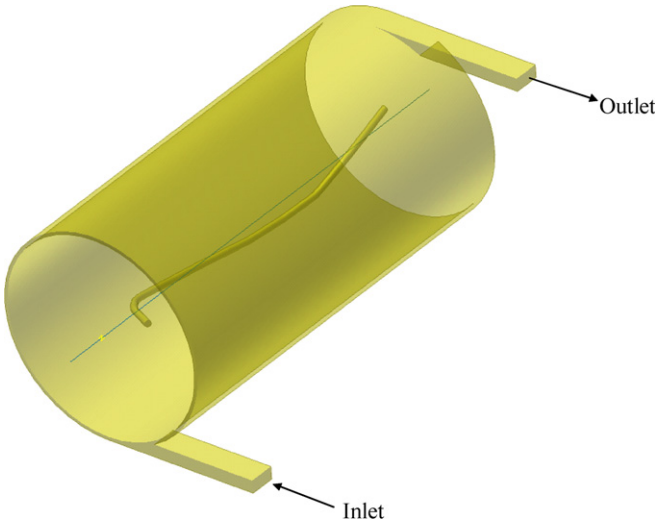

Fig. 12. 3-D view of the vortex core from computations for $h/D = 1/16$, $Re = 18{,}000$ and $L/D = 2$. The vortex center moves around the spiraling helix shown in the figure.

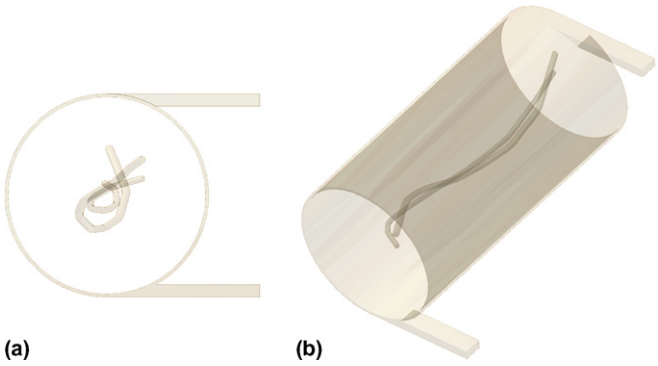

Fig. 13. Comparison of the vortex core movement for the case with $h/D = 1/16$, $L/D = 2$ and (a) $Re = 9000$ (outer locus), (b) $Re = 18{,}000$ (inner locus). The vortex core shows a distinct tendency to fling out of the centerline at lower Reynolds number.

the vortex centers have been traced out in Fig. 13. The parameter used for comparison here is the Reynolds number and its effect on the deviation of the vortex from the axis of the cylinder has been studied. It was found that at a high Reynolds number, the vortex core shifts towards the axis of the cylinder as compared to the case with the lower Reynolds number. The vortex meandering around the axis tends to reach self-similarity with increasing the Reynolds number, and vortex core meandering is at a minimum.

Finally, a quantitative comparison between the standard k–ε and the RNG k–ε model was done to understand the turbulence decay along the cylinder. Legrand et al. (2000) had found that energetic structures that were detected in the vicinity of the inlet rapidly decay along the flow path because of the decrease in swirl intensity. On the same lines, in the present study it was found numerically that the RNG k–ε model predicted a higher decay in the average turbulence intensity as compared to the standard k–ε model, as is shown in Fig. 14. The turbulence intensity is defined as the ratio of the root mean-square turbulent velocity fluctuation to the mean flow velocity (u'/U), generally expressed as a percentage. If the turbulence kinetic energy at any particular plane be computed, it can be found to obey the relationship $k = 3(UI)^2/2$, where 'I' is the turbulence intensity. For the comparison of RNG k–ε and the standard k–ε model the inlet turbulence intensity was kept the same. Turbulence, in general, is affected by

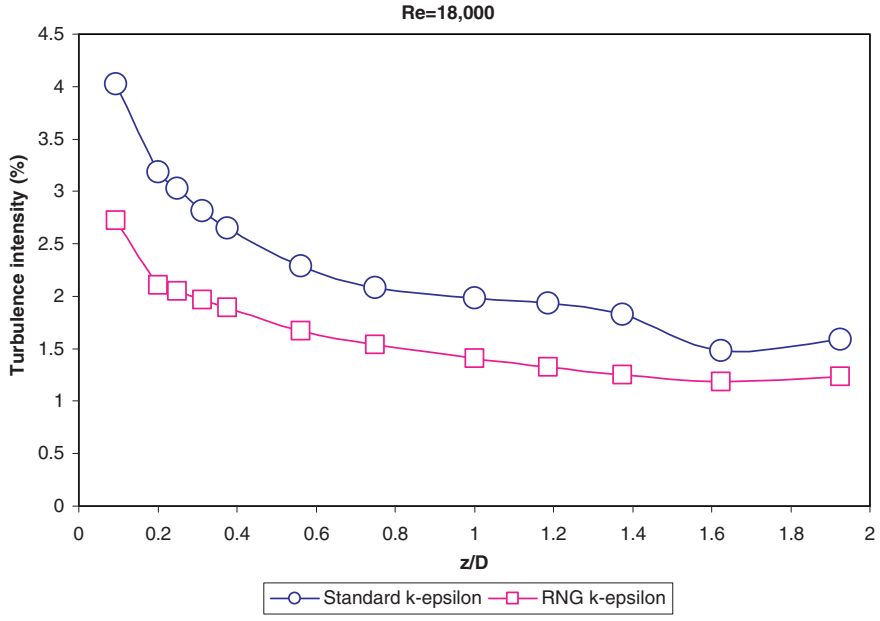

Fig. 14. Variation of the average turbulence intensity (in %) on different planes normal to the axis of the cylinder for the k–ε and the RNG k–ε models at $Re = 18{,}000$.

rotation or swirl in the mean flow. The RNG model provides an option to account for the effect of swirl or rotation by modifying the turbulence viscosity appropriately. Thus, the larger decay could be accounted for the fact that in the RNG model, because of the swirl modification factor, the turbulence in the flow gets uniformly distributed in the cylinder as compared to the standard k–ε model.

5. General flow structure and summary

Based on various snapshots of velocity vectors in the cylinder from both PTV experiments and three-dimensional computations using the RNG k–ε model, a general picture of the flow emerges. The flow spirals along the cylinder wall making a helical pattern that appears to be close to a theoretical helix. The velocity vectors for this flow are generally large and predominantly in the positive direction towards the exit. A secondary flow consists of two cells that are clockwise, appearing in two skewed planes. Tangential velocity results from the PTV experiments and computations were compared and found to be in reasonably good agreement. Results were also compared for different inlet height to cylinder diameter ratios at the same Reynolds number and it was found that the vortex center follows a similar path en route to the exit, although the vortex centers are not present at the same locations. It was found that for the situations involving highly swirling flows, the RNG k–ε model predicted much more accurate results than the standard k–ε model.

The results described predict some problems for using this cyclone as for centrifugal separation. First, a small part of the inlet stream proceeds in a single helix to the outlet port. The outlet, on the other hand, had been actually placed to minimize this since the helix appeared to end 180° away from it azimuthally, but some of the stream avoided the recirculating secondary flow and escaped. This implies that some of the pumped-in fluid had only a minimal residence time for separation. Also, the exit plane end of the vortex center resided near the outlet, so the separated light phase could be returned to the mixture through the outlet. Secondly, axial acceleration and warping of the vortex were present in the flow. This three-dimensionality is a major deviation from the ideal model. It can only be expected to encourage mixing, reduce the separating efficiency and hinder the light phase retention of the cyclone.

Acknowledgements

Thanks are due to Dr. T.A. Conover and Mr. Yong Pan for help with the experimental and numerical analysis.

Appendix A. Two-equation turbulence models

Launder and Spalding (1974) developed the well-known standard k–ε model. In formulating the k–ε model, the Reynolds-stress tensor is used. In case of the Boussinesq approximation being valid, the Reynolds-stress tensor is given by

$$\tau_{ij} = 2\nu_T S_{ij} - \frac{2}{3}k\delta_{ij} \tag{A.1}$$

where S_{ij} is the mean strain-rate tensor given by

$$S_{ij} = \frac{1}{2}\left(\frac{\partial u_i}{\partial x_j} + \frac{\partial u_j}{\partial x_i}\right) \tag{A.2}$$

Using the transport equations for k and ε and through certain closure conditions, the standard k–ε model is deduced.

Kinematic eddy viscosity

$$\nu_T = C_\mu \frac{k^2}{\varepsilon} \tag{A.3}$$

Turbulence kinetic energy

$$\frac{\partial k}{\partial t} + U_j\frac{\partial k}{\partial x_j} = \tau_{ij}\frac{\partial U_i}{\partial x_j} - \varepsilon + \frac{\partial}{\partial x_j}\left[\left(\nu + \frac{\nu_T}{\sigma_\varepsilon}\right)\frac{\partial k}{\partial x_j}\right] \tag{A.4}$$

Dissipation rate

$$\frac{\partial \varepsilon}{\partial t} + U_j\frac{\partial \varepsilon}{\partial x_j} = C_{\varepsilon_1}\frac{\varepsilon}{k}\tau_{ij}\frac{\partial U_i}{\partial x_j} - C_{\varepsilon_2}\frac{\varepsilon^2}{k} + \frac{\partial}{\partial x_j}\left[\left(\nu + \frac{\nu_T}{\sigma_\varepsilon}\right)\frac{\partial \varepsilon}{\partial x_j}\right] \tag{A.5}$$

What differentiates the different forms of the k–ε turbulence models is the way the closure conditions are defined and coefficients computed.

References

Choudhury, D., 1993. Introduction to Renormalization Group Method and Turbulence Modeling. Fluent Inc. Technical Memorandum TM-107.

Durst, F., Wennerberg, D., 1991. Numerical aspects of calculation of confined swirling flows with internal recirculation. Int. J. Numer. Methods Fluids 12, 203–224.

Hedlund, C.R., Ligrani, P.M., 2000. Local swirl chamber heat transfer and flow structure at different Reynolds numbers. Trans. ASME J. Turbomach. 122 (2), 375–385.

Imaichi, K., Ohmi, K., 1983. Numerical processing of flow visualization pictures – measurement of two-dimensional vortex flow. J. Fluid Mech. 129, 283–311.

Jakirilić, S., Hanjalic, K., Tropea, C., 2002. Modeling rotating and swirling turbulent flows: a perpetual challenge. AIAA J. 40 (10), 1984–1996.

Khalighi, B., 1989. Study of the intake swirl process in an engine using flow visualization and particle tracking velocimetry. In: Flow Visualization, FED-vol. 85, ASME Winter Annual Meeting, San Francisco, pp. 37–47.

Khalighi, B., Lee, Y.H., 1989. Particle tracking velocimetry: an automatic image processing algorithm. Appl. Opt. 28 (20), 4328–4332.

Kumar, R., Conover, T.A., 1993. Flow visualization studies of a swirling flow in a cylinder. J. Exp. Thermal Fluid Sci. 7, 254–262.

Launder, B.A., Spalding, D.B., 1974. The numerical computation of turbulent flows. Comput. Methods Appl. Mech. Eng. 3 (269), 269–289.

Legrand, J., Legentilhomme, P., Lefebvre, G., 2000. Analysis of wall turbulence in swirling annular decaying flow induced by a tangential fluid inlet. Can. J. Phys. 78 (8), 779–801.

Mikulec, A., Kent, J.C., Adamczyk, A.A., Rimai, L., 1988. Effects of intake port configuration on induction-generated swirl in a piston engine: a water analog experiment using particle tracking velocimetry.

Int. Symp. Fluid Control Measurement Mechanics and Flow Visualization. Sheffield University, England, pp. 50–54.

Neto, S.R.D., Legentilhomme, P., Legrand, J., 1998. Finite-element simulation of laminar swirling decaying flow induced by means of a tangential inlet in an annulus. Comput. Methods Appl. Mech. Eng. 165 (1–4), 189–213.

Pan, Y., 1992. Numerical study of a three-dimensional swirling flow in a cylinder. M.S. Thesis. Mechanical Engineering, Clemson University.

Parks, S.M., Oluwole, O., Wehbe, W.I., Olson, T.J., Petty, C.A., 2002. The influence of hydrocyclone geometry on separation performance. In: Proceedings of Minerals Engineering Conference on Solid–Liquid Separation, Falmouth, UK, June 18–20.

Patankar, S.V., 1980. Numerical Heat Transfer and Fluid Flow. Taylor and Francis.

Pettersson, B.A., Andersson, H.I., Brunvoll, A.S., 1998. Modeling near-wall effects in axially rotating pipe flow by elliptic relaxation. AIAA J. 36 (7), 1164–1170.

Sharif, M.A.R., Busnaina, A.A., 1988. Modeling of three-dimensional swirling flow in cylindrical configurations. In: Tippins, V.A., Patton, E.M. (Eds.), Proceedings of the ASME International Computers in Engineering Conference, San Francisco, California, vol. 3, pp. 455–463.

Svarovsky, L., 1985. Solid–liquid separation processes and technology. In: Williams, J.C., Allen, T. (Eds.), Handbook of Powder Technology, vol. 5. Elsevier Publishing Company.

Walter, J.A., 1989. Development of a quantitative velocity imaging system and its application to offset channel flow. M.S. Thesis. Mechanical Engineering, University of Iowa.

Yakhot, V., Orszag, S.A., 1986. Renormalization group analysis of turbulence. J. Sci. Comput. 1 (3).

Yang, X.D., Ma, H.Y., 2003. Computation of strongly swirling confined flows with cubic eddy-viscosity turbulence models. Int. J. Numer. Methods Fluids 43 (12), 1355–1370.